Journal of Power Sources 205 (2012) 173–179

Contents lists available at SciVerse ScienceDirect

Journal of Power Sources

journal homepage: www.elsevier.com/locate/jpowsour

Tailored heat transfer characteristics of pelletized $LiNH_2$–MgH_2 and $NaAlH_4$ hydrogen storage materials

Carsten Pohlmann[a], Lars Röntzsch[b,*], Jianjiang Hu[c], Thomas Weißgärber[b], Bernd Kieback[a,b], Maximilian Fichtner[c]

[a] Institute for Materials Science, Technische Universität Dresden, Helmholtzstr. 7, 01069 Dresden, Germany
[b] Fraunhofer Institute for Manufacturing Technology and Advanced Materials, Branchlab Dresden, Winterbergstr. 28, 01277 Dresden, Germany
[c] Karlsruhe Institute of Technology, Institute of Nanotechnology, 76021 Karlsruhe, Germany

ARTICLE INFO

Article history:
Received 7 September 2011
Received in revised form 4 January 2012
Accepted 6 January 2012
Available online 16 January 2012

Keywords:
Sodium alanate
Lithium amide
Magnesium hydride
Expanded natural graphite
Thermal conductivity
Heat transfer

ABSTRACT

Complex hydrides are attractive candidates for solid-state hydrogen storage because of their high hydrogen storage capacities and moderate operation temperatures. However, the fast and efficient transport of reaction heat through the hydride bed is an unsolved problem due to the low intrinsic heat conductivities of complex hydrides.

Here, we report on increasing the effective thermal conductivities of a $NaAlH_4$- and a $LiNH_2$–MgH_2-based material by admixing expanded natural graphite (ENG) up to 25 mass% and compaction with up to 400 MPa. Thermal conductivities in radial and axial direction, microstructure and phase fractions of these pellets were determined. With increasing ENG content the heat transfer characteristics of both systems were enhanced from less than 1 $W\,m^{-1}\,K^{-1}$ up to 38 $W\,m^{-1}\,K^{-1}$. The pelletized hydride–graphite composites can be processed easily and safely compared to loose powders. Further, they have increased volumetric storage capacities of up to 59 g-H_2 l^{-1} and 54 g-H_2 l^{-1} compared to the loose powders with 19 g-H_2 l^{-1} and 18 g-H_2 l^{-1} for the $NaAlH_4$- and a $LiNH_2$–MgH_2-based material, respectively, and they are very suitable for a tubular hydride tank design due to anisotropic heat transfer characteristics.

1. Introduction

Establishing a hydrogen-based energy cycle is one option of ensuring a safe, environmentally friendly and sustainable energy distribution [1]. However, the compact and efficient storage of the energy carrier is still an unsolved problem [2]. Major research activity is being carried out in the field of solid-state hydrogen storage, e.g. in order to meet the ambitious targets of the US Department of Energy (DoE) regarding hydrogen storage density, kinetics, safety, efficiency and materials costs [3]. In recent years, light complex hydrides have been of growing interest due to their high gravimetric as well as volumetric hydrogen storage densities at moderate ab-/desorption temperatures. Promising candidates have been identified such as alanates and amides of light weight metals like Na and Li [4–6].

In order to tailor the hydrogenation and dehydrogenation kinetics of complex hydrides, numerous groups have studied the effects of catalytically active species such as transition metals or transition metal compounds (e.g. halides) which are admixed by high-energy ball-milling [7–10]. Furthermore, it has been established that various hydrogen storage materials with a nano-scale microstructure (grain size of 100 nm and less) exhibit faster kinetics for hydrogen sorption reactions compared to coarse grained materials [4,11,12].

Considering real-sized storage tanks based on hydrides, the transfer of the heat from the reaction enthalpy during hydrogenation and dehydrogenation was found to limit the rapid hydrogen loading and unloading of the tank [13,14]. To overcome these limitations, the heat transfer characteristics of hydride beds have to be enhanced. Typical values for the thermal conductivity of granular hydride beds are in the range of 1 $W\,m^{-1}\,K^{-1}$ and less [15]. There are various studies in the literature devoted to that matter [13,16–26]. For example, there are reports on auxiliary heat exchanging capillary tubes inside the hydride bed [13]. Others integrated the storage material into auxiliary cellular metal structures with high thermal conductivity [18,21,25]. Alternatively, hydride–graphite composites with increased effective thermal conductivity were investigated [19,20,22,24]. Hydride–graphite composites allow to tailor the thermal conductivity very accurately and to create anisotropic heat conduction properties. For example, in previous works it was found that the thermal conductivity of a compacted magnesium hydride-based system can be controlled in a wide range from 1 $W\,m^{-1}\,K^{-1}$ up to 47 $W\,m^{-1}\,K^{-1}$ and to align the graphite perpendicular to the direction of compaction [19,22]. The aligned graphite layers result in a strongly increased thermal conductivity

* Corresponding author. Tel.: +49 351 2537 411; fax: +49 351 2537 399.
E-mail address: Lars.Roentzsch@ifam-dd.fraunhofer.de (L. Röntzsch).

0378-7753/$ – see front matter © 2012 Elsevier B.V. All rights reserved.
doi:10.1016/j.jpowsour.2012.01.064

in radial direction. This is beneficial for the preferred tubular tank design where almost the entire reaction enthalpy is transported in radial direction [27]. Moreover, a constant effective thermal conductivity of pelletized hydrogen storage materials independent of its state of hydrogenation may be achieved as showed earlier [22].

The goal of this study is to demonstrate the enhancement of the effective thermal conductivity in pelletized mixtures of complex hydrides and expanded natural graphite (ENG). In contrast to our previous work [22], where melt-spun magnesium alloy flakes (metallic state) were used, here we start from powdery hydrides (hydrogenated state). Due to different production processes of these materials, their particle shape and size differ strongly: The melt-spun Mg alloys consist of chopped flakes (platelets with dimensions of 1 mm × 1 mm × 40 μm approximately). In contrast, ball-milled complex hydride powders have typical particle sizes in the range of several micrometers. Moreover, starting from the metallic state requires different pellet porosity than starting from the hydrogenated state with hydride powders because of the volume changes during hydrogenation/dehydrogenation. The residual open porosity inside the pelletized hydrogen storage material needs to be optimized in view of two major requirements: On the one hand these pellets should result in a volumetric hydrogen storage capacity significantly higher than that of loose powders or flakes. On the other hand, the flow of gaseous hydrogen through the pellet should still be possible. In short, these issues require different compaction parameters which cause a different phase distribution and phase alignment inside the pellets which in return should result in different heat conduction characteristics. Despite these differences, the target of this and our former study [22] is similar, namely to increase the effective heat conduction inside the reaction bed to rapidly transport the reaction enthalpies during hydrogenation/dehydrogenation.

In that respect, two prominent complex hydride materials systems have been examined to understand the effects of compaction and graphite addition. Although the respective catalyst species do not represent the optimal choice concerning hydrogenation and dehydrogenation kinetics, the compaction behavior, hydride and graphite phase alignment as well as thermal conductivity are not influenced due to their low molar fraction. The two systems under study are: $NaAlH_4$ doped with 4 mol% $CeCl_3$ and a 2:1 molar mixture of $LiNH_2$ and MgH_2. The molar ratio of 2:1 is chosen because it has been found to be the optimal composition in terms of hydrogen storage capacity and ammonia generation based on our previous research [28]. As discussed in our previous work, the effective thermal conductivity within the hydride bed should be in the range between 10 W m^{-1} K^{-1} and 20 W m^{-1} K^{-1} in radial direction if a tubular storage tank with an inner diameter between 30 and 50 mm is assumed [22]. Regarding $NaAlH_4$-based tanks, Raju and Kumar found that an optimal effective thermal conductivity of approximately 8 W m^{-1} K^{-1} is required for a tank with internal heat exchanging elements (aluminum fins and cooling/heating tubes) [23].

Furthermore, the compaction of those highly reactive complex hydride–ENG mixtures into pellets is demonstrated in this contribution under quasi-inert conditions using a state-of-the art uniaxial 10-ton press. Suchlike pelletized specimens of both $NaAlH_4$- as well as $LiNH_2$–MgH_2-based systems are exemplarily shown in Fig. 1. Due to compaction, the reactivity of these materials with oxygen and humidity is drastically reduced which allows easier and safer handling. Moreover, the volumetric hydrogen storage capacities of pelletized hydrogen storage materials are increased compared to powdery hydride beds which results in a higher mass ratio between the hydride material and the tank as demonstrated recently [29,30].

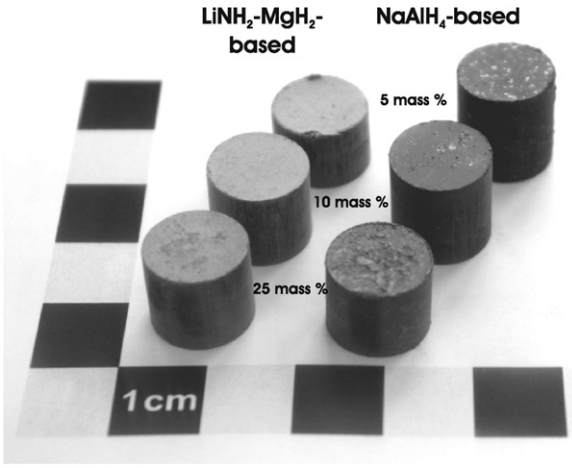

Fig. 1. Pellets of both material systems for various ENG contents compacted at 300 MPa.

2. Experimental

In this work, two materials systems have been studied:

System 1: $NaAlH_4$ (doped with 4 mol% $CeCl_3$)
System 2: $LiNH_2$–MgH_2 with a mol ratio of 2:1

The starting materials were acquired commercially: $LiNH_2$ (>95%) from Sigma–Aldrich, MgH_2 (98%) from Alfa Aesar, $NaAlH_4$ (96%) from Albemarle Corporation and $CeCl_3$ (99.5%) from Alfa Aesar (purities in brackets are given by the manufacturers). The powders were ball-milled according to the system composition. Ball milling was performed in a Retsch PM 400E with a powder-to-ball weight ratio of 1:90 in a 250 ml milling jar of stainless steel at a revolution speed of 200 rpm for 20 h. Three different types of stainless steel balls were used: one with 20 mm, four with 15 mm and six with 13 mm in diameter.

The as-milled powders have been examined by X-ray diffraction (XRD, Bruker AXS: D8 ADVANCE) using Cu Kα radiation in the angular range between 25° and 65° (2Θ). During XRD analysis, the powders were protected from the atmosphere using a kapton foil.

The milled powders were thoroughly mixed with ENG (delivered by SGL Carbon) in argon atmosphere (99.998% Ar) using a tubular mixer (Turbula T2F). Various ENG contents of 0 mass%, 5 mass%, 10 mass% and 25 mass% were chosen for the mixture with both hydride systems.

After mixing, the powder-ENG blends were compacted into cylindrical pellets with 12 mm in diameter using a TIRA test 2300. Due to the high reactivity of both hydride systems the compaction process was performed under Ar atmosphere. Thus, a glove box-like processing chamber has been installed at the uniaxial 10-ton press with a constant flow of argon of 300 l h^{-1} (cf. Fig. 2a). Three compaction pressures of 200 MPa, 300 MPa and 400 MPa were chosen, where optimal porosity is anticipated [22]. The densities of the pellets (pellet mass divided by its volume) were determined in order to retrieve the residual porosity within the pellets taking the intrinsic densities of each material into account. The theoretical density of ENG of about 2.14 g cm^{-3} was measured with a pycnometer (AccuPyc 1330). The theoretical densities of both hydride systems were determined using a magnetic suspension balance (Rubotherm), where the sample weight was measured at different inert gas pressures. Due to buoyancy it is, thereby, possible to determine volume and mass of the hydride materials [31]. From that we derived the densities of the $NaAlH_4$- and the $LiNH_2$–MgH_2-system which amount to 1.58 g cm^{-3} and 1.45 g cm^{-3}, respectively.

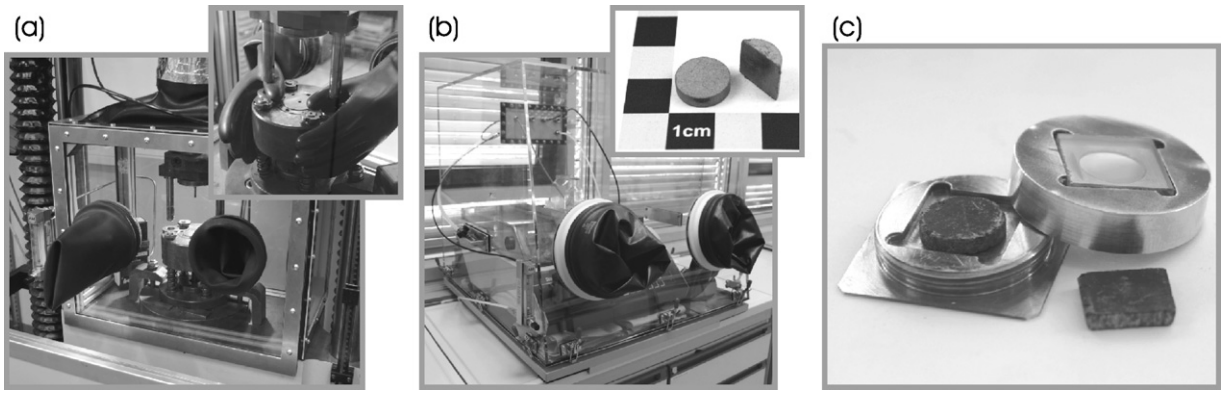

Fig. 2. Inert processing chain for the characterization of the $NaAlH_4$- and $LiNH_2$–MgH_2-based systems; (a) chamber of the uniaxial press, (b) glove box for the Accutom 5 cutting device (with examples of cut $LiNH_2$–MgH_2-based pellets with 5 mass% ENG), (c) measuring cell for Netzsch LFA 447 NanoFlash (with examples of slices for the determination of axial and radial thermal conductivity).

In order to measure the axial as well as the radial thermal conductivity of the pellets, the Accutom 5 cutting device was placed inside a glove box filled with an argon atmosphere (99.998% Ar; cf. Fig. 2b). Afterwards, the temperature diffusivities of the slices (uncertainty of 3% given by the manufacturer) were determined using a self-designed measuring cell which suits the Netzsch LFA 447 NanoFlash (cf. Fig. 2c). The respective thermal conductivity was calculated by multiplying temperature diffusivity, density and specific heat capacity. The specific heat capacity was determined using differential scanning calorimetry (Netzsch DSC 204 F1 Phoenix) with an uncertainty of 3% (value given by the manufacturer). Furthermore, radial cross-sections of each specimen were prepared for metallographic inspection. Due to the high reactivity of the specimens with humidity and oxygen, the pellets were prepared using an oil-based grinding and polishing fluid. Directly after cleaning with heptane, the surface was covered with silicon oil to prevent subsequent oxidation. The microscopic examination was carried out using an Olympus Laser Microscope OLS4000 where the sample could be placed in an upright position.

All measurement errors were calculated using the law of error propagation. The total measurement errors are given by error bars in the graphs.

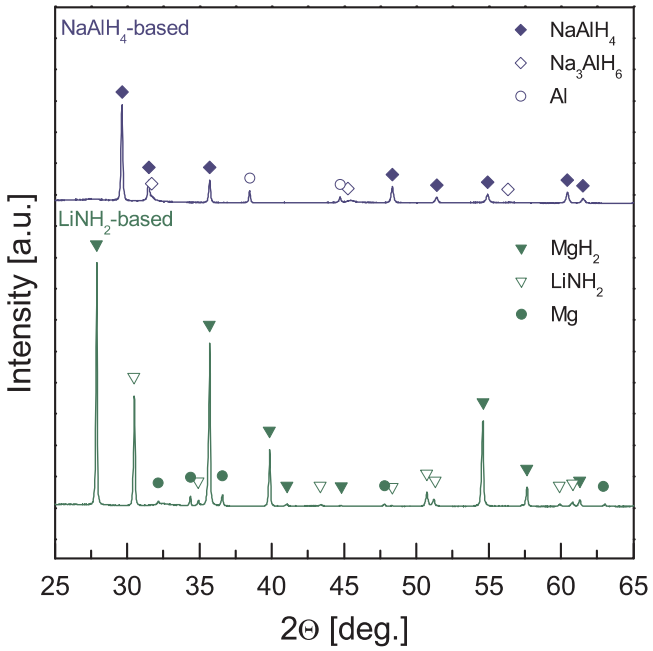

Fig. 3. X-ray diffraction patterns of the $NaAlH_4$- and $LiNH_2$–MgH_2-based powders in the as-milled state.

3. Results and discussion

3.1. Phase composition of the initial powders

Fig. 3 presents the X-ray diffraction patterns of the two systems (system 1: $NaAlH_4$ doped with 4 mol% $CeCl_3$; system 2: $LiNH_2$–MgH_2 with a mol ratio of 2:1) in the as-milled state without graphite (see Section 2). Accordingly, system 1 exhibits three phases: $NaAlH_4$, Na_3AlH_6 and metallic Al. In system 2, $LiNH_2$, MgH_2 and metallic Mg have been detected. Evidently, both systems exhibit residual metallic phases of comparably low intensities. In the case of system 1, some of the sodium alanate is dehydrogenated during high energy ball milling in the presence of the catalyst which explains the presence of metallic Al after milling. The diffraction reflexes of the metallic Mg in system 2 originate from the starting material which is caused by incomplete hydrogenation during manufacturing of the powdery MgH_2 (see Section 2). The presence of those metallic phases, however, does not influence the materials processing. Due to the low molar ratio of the residual metallic phases their influence on the thermal conductivities of the pellets is insignificant.

3.2. Phase fractions of the hydride–ENG pellets

Table 1 presents the volume fractions of the residual porosity, the hydride and the ENG phase inside the pellets. These values have been determined for different ENG contents and compaction pressures for both systems. It has to be noted that both systems without ENG could only be compacted into pellets with a thickness up to 1.5 mm. Thicker pellets disintegrated due to internal stresses and wall friction during removal from the die. The role of ENG during the compaction process is twofold: At first, it acts as lubricant and binding agent which results in a better compressibility of the hydride–ENG powder mixture. Secondly, during withdraw of the compacted pellet from the die, ENG causes a more intense axial spring back effect due to an internal volume relaxation of the graphite layers which are orientated perpendicular to the direction of compression. Therefore, an increase in ENG content can result in either a lower or higher porosity volume fraction depending on which effect dominates.

In system 1, the residual porosity decreases with increasing compaction pressure as expected. For example, a decrease of the

Table 1
Phase fraction of the $NaAlH_4$- and the $LiNH_2$–MgH_2-based pellets for various ENG contents and compaction pressures.

Material	ENG content [mass%]	Compaction pressure [MPa]	Porosity [vol.%]	Absolute error [vol.%]	ENG content [vol.%]	Absolute error [vol.%]	Hydride volume fraction [vol.%]	Absolute error [vol.%]
System 1: $NaAlH_4$-based	5	200	24.5	1.4	2.8	0.4	72.7	1.7
		300	20.4	1.2	3.0	0.4	76.6	1.6
		400	17.5	1.1	3.1	0.4	79.4	1.5
	10	200	24.9	0.8	5.7	0.5	69.4	1.4
		300	20.2	1.1	6.1	0.7	73.7	1.8
		400	20.5	2.1	6.1	1.0	73.5	3.0
	25	200	24.9	1.4	15.2	1.6	59.9	3.0
		300	23.0	2.3	15.6	2.3	61.4	4.6
		400	19.9	2.0	16.2	2.4	63.9	4.4
System 2: $LiNH_2$–MgH_2-based	5	200	31.1	0.8	2.4	0.2	66.5	0.9
		300	30.4	0.9	2.4	0.2	67.2	1.1
		400	31.9	1.0	2.3	0.2	65.8	1.2
	10	200	31.8	0.2	4.8	0.2	63.4	0.5
		300	30.3	0.7	4.9	0.3	64.8	1.0
		400	28.0	0.4	5.1	0.3	67.0	0.7
	25	200	29.5	1.0	13.3	0.8	57.2	1.8
		300	26.7	1.4	13.8	1.1	59.4	2.5
		400	25.3	0.7	14.1	0.8	60.6	1.6

residual porosity from about 25 vol.% to about 17–20 vol.% for compaction pressures of 200 MPa and 400 MPa can be noticed according to Table 1. However, an increasing ENG content does not result in smaller porosity fractions inside the pellets. Indeed, a small increase in porosity for a higher ENG content was observed (for example at 300 MPa: 20.4 vol.% porosity for 5 mass% ENG vs. 23.0 vol.% porosity for 25 mass% ENG). Already at low amounts of ENG system 1 can be compressed to low porosities, therefore, any further increase in ENG content results in no significant increase in compressibility.

In system 2, the pellets have generally higher porosity fractions compared to system 1 which suggests a lower compressibility of the $LiNH_2$–MgH_2 powder mixture compared to the $NaAlH_4$ powder. At a low ENG content of 5 mass%, an increase of the compaction pressure does not lead to a pronounced decrease of the residual porosity. At higher ENG contents, however, a clear decrease of the porosity fraction was observed, for example, for 25 mass% ENG residual porosities of 29 vol.%, 27 vol.% and 25 vol.% were found for compaction pressures of 200 MPa, 300 MPa and 400 MPa, respectively. Here, in contrast to system 1, the lubricant and binding effect of ENG in $LiNH_2$–MgH_2–ENG mixtures is stronger than the spring back effect after withdrawal of the pellets from the die due to the lower compressibility of the $LiNH_2$–MgH_2-based powders.

Furthermore, knowing the volume fractions of all phases present (hydride, ENG and porosity) one can calculate both volumetric and gravimetric storage densities of suchlike prepared pellets. For this purpose the storage densities of the according hydride are multiplied by its mass and volume fraction in the pellet to retrieve the maximum gravimetric and volumetric hydrogen storage density, respectively. For $NaAlH_4$ a theoretical gravimetric storage density of 5.6 mass%-H_2 is assumed taking the following two step reactions (1) and (2) into account [32]:

$$3NaAlN_4 \rightleftarrows Na_3AlH_6 + 2Al + 3H_2 \quad (1)$$

$$Na_3AlH_6 \rightleftarrows 3NaH + Al + (3/2)H_2 \quad (2)$$

Doping $NaAlH_4$ with 4 mol% $CeCl_3$ reduces the theoretical gravimetric storage density to 4.7 mass%-H_2. According to Dolotko et al. [33] the $LiNH_2$–MgH_2 mixture (2:1) releases hydrogen as stated in reaction (3), where an initial dehydrogenation takes place followed by the actual reversible process upon further cycling.

$$2LiNH_2 + MgH_2 \rightarrow Li_2Mg(NH)_2 + 2H_2 \rightleftarrows Mg(NH_2)_2 + 2LiH \quad (3)$$

The reversible hydrogenation is a two step reaction [34] with a theoretical gravimetric storage density of 5.6 mass%-H_2.

The theoretical volumetric storage densities of the materials are determined by multiplying the gravimetric densities with the theoretical mass density of the corresponding hydride. This results in 74 g-H_2 l^{-1} and 81 g-H_2 l^{-1} for systems 1 and 2, respectively. Based on that, the storage densities of the actual pellets containing porosity can be calculated. Those values are plotted in Fig. 4. It should be noted that for both systems the expected trend holds true, i.e. with increasing compaction pressure the volumetric storage density increases, too. The only exception was found in system 2 for 5 mass% ENG and a compaction pressure of 400 MPa where a slightly higher fraction of residual porosity than expected was present (cf. porosity data with Table 1).

In order to compare the storage densities of such pellets with commonly used loose powders, the apparent density of the loose powders was determined according to DIN ISO 3923/1. As a result, a powder volume fraction of only about 26 vol.% and 22 vol.% was found which results in a volumetric storage density of 19 g-H_2 l^{-1} and 18 g-H_2 l^{-1} of the $NaAlH_4$- and $LiNH_2$–MgH_2-based powders, respectively. These values illustrate the enormous advantage of compaction regarding volumetric hydrogen storage density (cf. Fig. 4). In this regard, it is worth noting that the 2010 DOE target

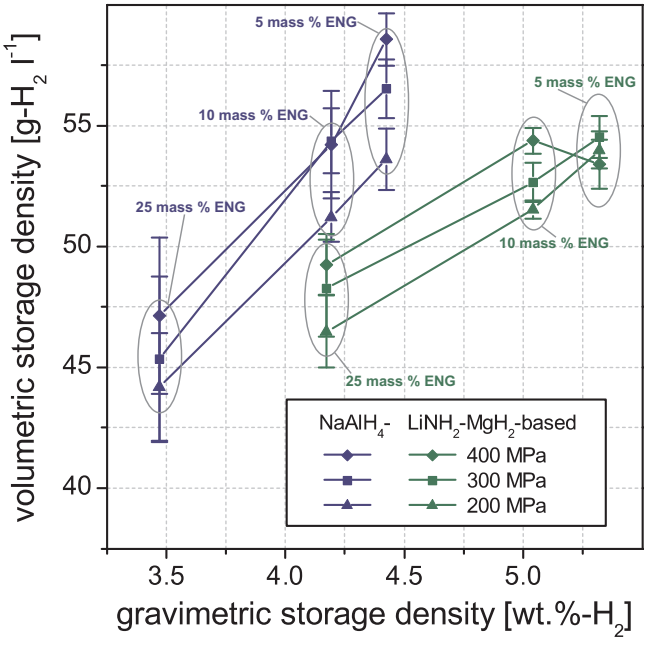

Fig. 4. Volumetric storage density vs. gravimetric storage density of the $NaAlH_4$-(blue) and $LiNH_2$–MgH_2-based (green) pellets at various ENG contents and compaction pressures. (For interpretation of the references to color in this figure legend, the reader is referred to the web version of this article.)

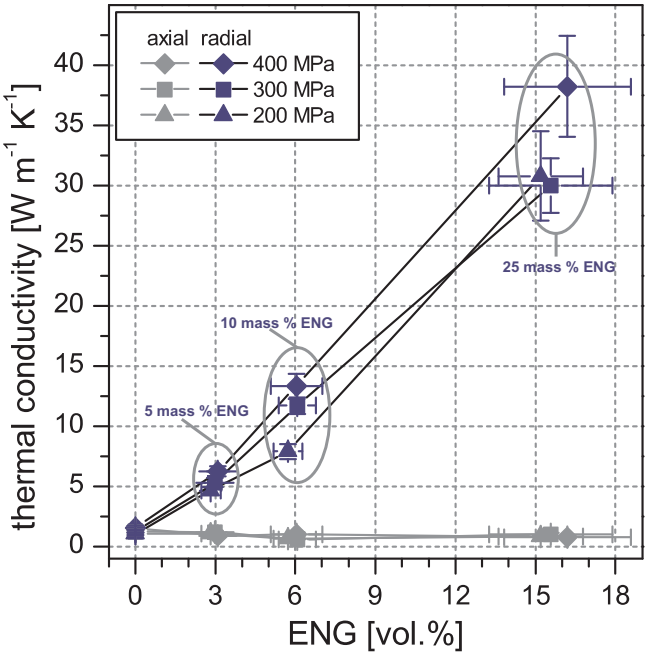

Fig. 5. Thermal conductivity in axial (gray) and radial (blue) direction vs. ENG content of the $NaAlH_4$-based pellets. (For interpretation of the references to color in this figure legend, the reader is referred to the web version of this article.)

for the volumetric system storage capacity of 28 g-H_2 l^{-1} cannot be met using loose hydride powders [3]. However, even by considering the lowest volumetric hydrogen capacity of all pellets investigated of 44 g-H_2 l^{-1} ($NaAlH_4$-based, 200 MPa, 25 mass% ENG), it is realistic to assume that a tank system on the basis of suchlike compacted hydride composites can fulfill this target. In view of the gravimetric DOE system targets, low ENG contents and a light weight construction would be most favorable. In this regard, $LiNH_2$–MgH_2 pellets with ENG contents below 10 mass% show the highest potential (cf. Fig. 4).

3.3. Heat conduction properties

The effective thermal conductivities of the $NaAlH_4$- and the $LiNH_2$–MgH_2-based pellets are presented in Figs. 5 and 6, respectively. The ENG content in the diagrams is given in volume percent of the porous compact since the effective thermal conductivity of a multi-component material is determined on the basis of the respective volume fractions. Due to decreasing porosity, the ENG volume fraction slightly increases with increasing compaction pressure (cf. Table 1). For example, the $NaAlH_4$- and $LiNH_2$–MgH_2-based specimens with an ENG content of 25 mass% compacted at 200–400 MPa have an ENG volume fraction from 15.2 to 16.2 and 13.3 to 14.1 vol.%, respectively.

From Figs. 5 and 6 it is evident that the thermal conductivities of the cylindrical pellets show a high degree of anisotropy regarding the heat flow perpendicular (radial) or parallel (axial) to the direction of compaction. Both systems exhibit a strong increase of their effective thermal conductivity in radial direction with increasing ENG content. They principally cover a similar range of approximately 2–40 W m^{-1} K^{-1} for ENG contents from 0–25 mass%. In contrast to that, the axial thermal conductivity remains at a low level (~1 W m^{-1} K^{-1}). Moreover, the slight variations of thermal conductivity of the pellets with equal ENG content but different compaction pressures (which refers to different fractions of residual porosity) indicate only a small influence of the porosity on the effective thermal conductivity. For example, at an ENG content of 5 mass% ENG the radial thermal conductivity varies between 4.6–6.2 W m^{-1} K^{-1} and 4.6–5.3 W m^{-1} K^{-1} for the $NaAlH_4$- and $LiNH_2$–MgH_2-based pellets, respectively. In our previous work powdery magnesium hydride admixed with the same ENG contents and compacted at similar pressures were investigated [22]. The MgH_2–ENG compacts covered a comparable range (about 1–43 W m^{-1} K^{-1}) and showed similar behavior (only slight dependence of porosity) in their effective radial thermal conductivity. Those findings suggest that the chosen hydride powders have no major influence on the

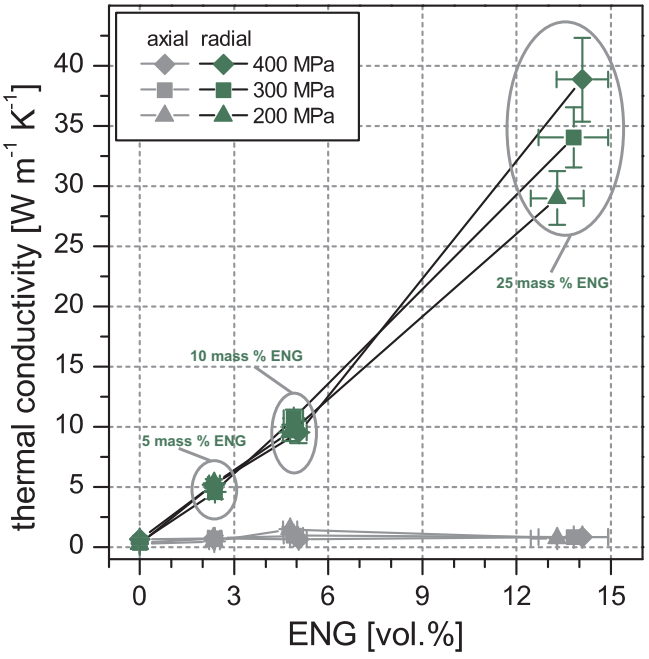

Fig. 6. Thermal conductivity in axial (gray) and radial (green) direction vs. ENG content of the $LiNH_2$–MgH_2-based pellets. (For interpretation of the references to color in this figure legend, the reader is referred to the web version of this article.)

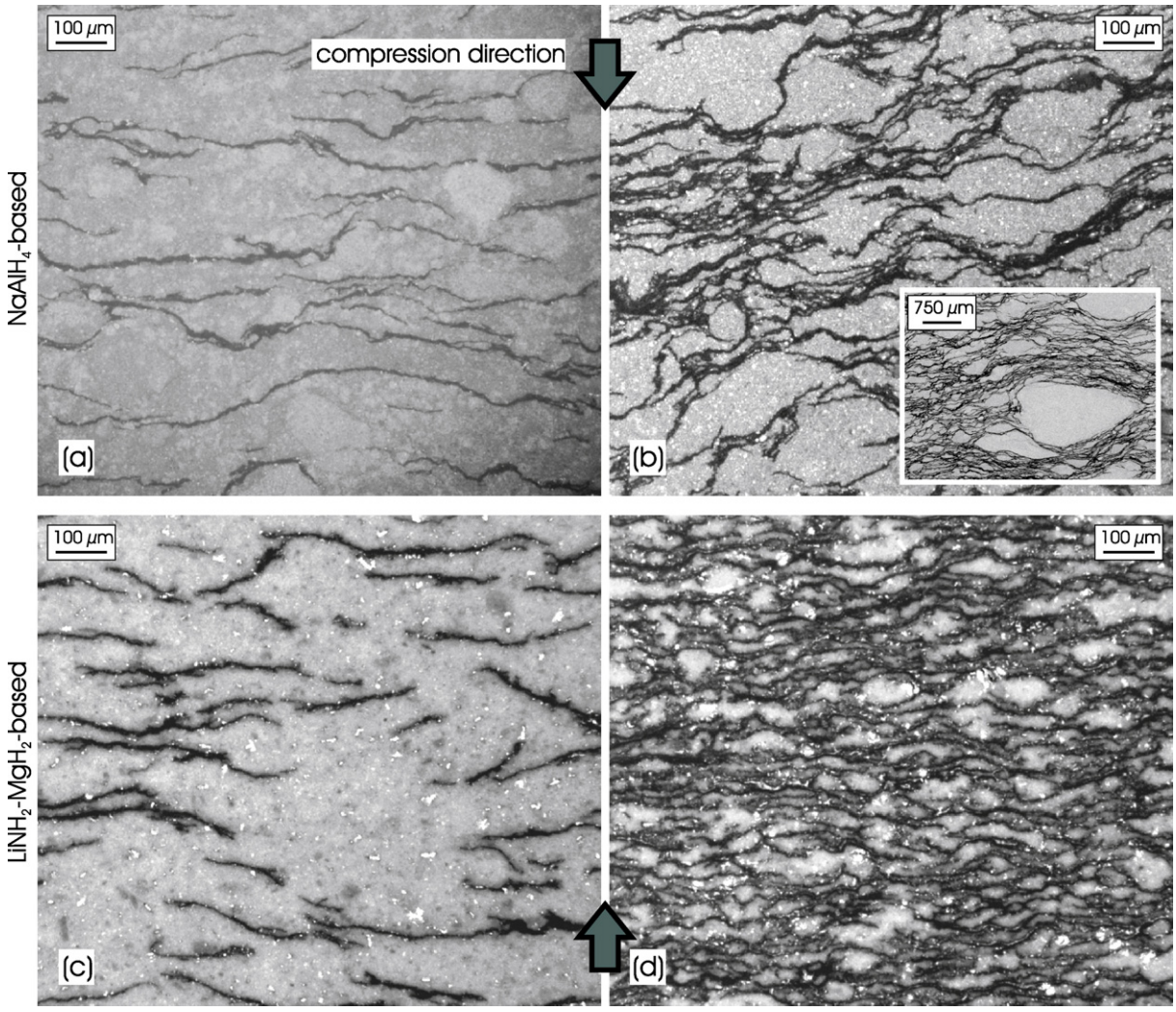

Fig. 7. Optical micrographs of the $NaAlH_4$- and the $LiNH_2$–MgH_2-based pellets with (a and c) 5 mass% and (b and d) 25 mass% ENG compacted at 200 MPa.

effective radial thermal conductivity of compacted hydride–ENG composites as long as the intrinsic heat conductivity of the hydride is much smaller than that of ENG. Consequently, the ENG content is a suitable control parameter to tune the thermal conductivity properties of pelletized hydride–ENG pellets in a wide range. It is demonstrated that the effective thermal conductivity in radial direction exceeds the stated target in the hydrogenated state and, thus, sufficient heat transfer during de- and rehydrogenation can be ensured. The geometrical integrity on cyclic dehydrogenation–rehydrogenation processing has to be investigated yet to guarantee a long material life time.

3.4. Microstructure and phase alignment

A cross-section optical micrograph of the $NaAlH_4$- and $LiNH_2$–MgH_2-based pellets with 5 mass% and 25 mass% ENG compacted at 200 MPa is given in Fig. 7. Here both hydride phases appear grayish, ENG is black and the very bright areas are metallic residues (aluminum or magnesium, respectively). Porosity may be present between hydride particles, at ENG–hydride phase boundaries as well as within the ENG. The spatial dimensions of the residual porosity cannot be resolved clearly in the optical micrographs because of the low contrast between porosity and ENG. Since the $NaAlH_4$-based specimens are very reactive at ambient conditions, it was not possible to avoid oxidation during preparation completely. Thus, the differently contrasted areas in Fig. 7a are assumedly slightly oxidized. However, the main focus is set on the distribution, shape and alignment of the ENG which is not affected by that.

The metallographic examination revealed that the distribution of ENG only insignificantly changes with increased compaction pressure. This is further supported by the small differences of the thermal conductivities of pellets with equal ENG content at various compaction pressures. Therefore, only micrographs of samples prepared at 200 MPa are presented here.

As suggested by the X-ray diffraction patterns, metallic residues are visible (aluminum and magnesium in the $NaAlH_4$- and $LiNH_2$–MgH_2-based systems, respectively). Again, due to possible oxidation in Fig. 7a the aluminum is not clearly visible.

From Fig. 7 it can be clearly seen that – as a general trend – ENG shows a strong anisotropic alignment, i.e. thin graphite veins perpendicular (radial) to the direction of compression are visible inside the hydride matrix. Furthermore, the connectivity between single ENG veins increases with increased ENG content. From the metallographic analysis, which provides a two dimensional impression of the hydride–ENG pellet, it can be deduced that a percolated network of graphite intercalating the whole pellet has been formed at 25 mass%. Considering the three dimensional structure of the pellet, however, it can be assumed that the percolation threshold is already reached at lower ENG contents. The heat can be

transported very fast within the ENG and therefore in radial direction which explains the strong anisotropy in heat conductivity shown in Figs. 5 and 6. Obviously, the ENG phase is the dominant factor to control the effective thermal conductivity of such composite pellets.

It should be noted that the $NaAlH_4$-based pellets with 25 mass% ENG show large ENG-free areas up to 1 mm in dimension (compare the inset in Fig. 7b). Thus, the mixing process was not sufficient for those high ENG contents apparently. Lower ENG contents did not show this effect. This could also explain the higher volume fractions of residual porosity found at those high ENG contents. It can be assumed further that local agglomeration of ENG will result in a stronger spring back during pellet withdraw. In this regard, a homogeneous ENG distribution is required. Moreover, a direct heat transfer from the hydride to the ENG network relies on a homogenous distribution of ENG, too. Since pellets with 25 mass% ENG strongly exceed the earlier stated target of 10–20 $W\,m^{-1}\,K^{-1}$ this effect is not of high importance for the preparation of hydride–ENG pellets. Yet, if ENG contents significantly higher than 10 mass% are required this effect needs to be investigated to ensure a homogeneous microstructure.

In future investigations a further important question needs to be addressed: How do phase alignment and phase distribution influence the cyclic dehydrogenation and rehydrogenation properties? In this regard, thermogravimetric experiments are under way using a specially designed pellet container to simulate given geometric confinements in a realistic tubular storage tank.

4. Conclusion

$NaAlH_4$ doped with 4 mol% $CeCl_3$ and a 2:1 molar mixture of $LiNH_2$ and MgH_2 were admixed with ENG and compacted into cylindrical pellets. Thereof, investigations regarding thermal conductivity, phase fraction and microstructure were conducted. Four different ENG contents of 0 mass%, 5 mass%, 10 mass% and 25 mass% were used at compaction pressures of 200 MPa, 300 MPa and 400 MPa. Because of pelletization a significant decrease of reactivity with air and humidity was achieved for both systems. Easier and safer handling as well as increased volumetric hydrogen storage capacities are clear advantages of the pelletized state. For example, the volumetric storage density of loose powders of 19 g-H_2 l^{-1} and 18 g-H_2 l^{-1} was increased to 59 g-H_2 l^{-1} and 64 g-H_2 l^{-1} by compaction of the $NaAlH_4$- and $LiNH_2$–MgH_2-based materials, respectively.

The compaction of complex hydrides without ENG was not possible for pellet heights larger than 1.5 mm due to the build-up of internal stresses during compaction. The ENG acts as lubricant during compaction and as a binding agent for the hydride powders and, therefore, dimensional stabilization of taller pellets is achieved.

Furthermore, it was demonstrated that ENG strongly improves the heat conduction properties of the investigated systems. It was found that ENG causes a strong anisotropy in thermal conductivity of the compacts. These findings are due to the fact that percolated graphite veins are oriented in radial direction preferably. For example, the thermal conductivity in radial direction of the $NaAlH_4$- and $LiNH_2$–MgH-based pellets compacted at 400 MPa could be advanced up to 38 $W\,m^{-1}\,K^{-1}$.

Acknowledgments

This work has been performed in the framework of the European Centre for Emerging Materials and Processes Dresden (ECEMP) which is funded by the European regional development fund and the Free State of Saxony. Furthermore, the authors would like to acknowledge financial support from the German-Chinese Sustainable Fuel Partnership project (contract no. 03BV108B) and the Fraunhofer Attract program. Experimental support by Mrs. K. Kümmel, Mrs. M. Eckhardt and Mr. Th. Hutsch is greatly acknowledged.

References

[1] P. Moriarty, D. Honnery, Int. J. Hydrogen Energy 34 (2009) 31–39.
[2] G. Principi, F. Agresti, A. Maddalena, S.L. Russo, Energy 34 (2009) 2087.
[3] US Department of Energy, Targets for On-Board Hydrogen Storage Devices. http://www1.eere.energy.gov/hydrogenandfuelcells/storage/current_technology.html (accessed July 2011).
[4] M. Fichtner, Adv. Eng. Mater. 7 (2005) 443–455.
[5] D.K. Ross, Vacuum 80 (2006) 1084–1089.
[6] U. Eberle, G. Arnold, R.v. Helmolt, J. Power Sources 154 (2006) 456–460.
[7] S. Barison, F. Agresti, S.L. Russo, A. Maddalena, P. Palade, G. Principi, G. Torzo, J. Alloy Compd. 459 (2008) 343–347.
[8] B. Bogdanovic, M. Felderhoff, A. Pommerin, F. Schüth, N. Spielkamp, Adv. Mater. 18 (2006) 1198–1201.
[9] O. Kircher, M. Fichtner, J. Alloy Compd. 404–406 (2005) 339–342.
[10] Y. Nakamori, G. Kitahara, K. Miwa, N. Ohba, T. Noritake, S. Towata, S. Orimo, J. Alloy Compd. 404–406 (2005) 396–398.
[11] M.U. Niemann, S.S. Srinivasan, A.R. Phani, A. Kumar, D.Y. Goswami, E.K. Stefanakos, J. Nanomater. 2008 (2008) 1–9.
[12] M. Fichtner, Zh. Zhao-Karger, J. Hu, A. Roth, P. Weidler, Nanotechnology 20 (2009) 204029–204034.
[13] M. Linder, R. Mertz, E. Laurien, Int. J. Hydrogen Energy 35 (2010) 8755–8761.
[14] M. Melnichuk, N. Silin, H.A. Peretti, Int. J. Hydrogen Energy 34 (2009) 3417–3424.
[15] K.J. Kim, M. Blanca, R. Arsenal, K.-H. Lee, Int. J. Hydrogen Energy 26 (2001) 609–613.
[16] F. Askri, M.B. Salah, A. Jemni, S.B. Nasrallah, Int. J. Hydrogen Energy 34 (2009) 6705–6711.
[17] M. Bhouri, J. Goyette, B.J. Hardy, D.L. Anton, Int. J. Hydrogen Energy 36 (2011) 621–633.
[18] M. Bhouri, J. Goyette, B.J. Hardy, D.L. Anton, Int. J. Hydrogen Energy 36 (2011) 6723–6738.
[19] A. Chaise, P.d. Rango, P. Marty, D. Fruchart, S. Miraglia, R. Olivès, S. Garrier, Int. J. Hydrogen Energy 34 (2009) 8589–8596.
[20] H.-P. Klein, M. Groll, Int. J. Hydrogen Energy 29 (2004) 1503–1511.
[21] S. Mellouli, H. Dhaou, F. Askri, A. Jemni, S.B. Nasrallah, Int. J. Hydrogen Energy 34 (2009) 9393–9401.
[22] C. Pohlmann, L. Röntzsch, S. Kalinichenka, T. Hutsch, B. Kieback, Int. J. Hydrogen Energy 35 (2010) 12829–12836.
[23] M. Raju, S. Kumar, Int. J. Hydrogen Energy 36 (2011) 1578–1591.
[24] A.R. Sánchez, H.-P. Klein, M. Groll, Int. J. Hydrogen Energy 28 (2003)515–527.
[25] S. Suda, Y. Komazaki, N. Kobayashi, J. Less Common Met. 89 (1983) 317–324.
[26] I. Utz, N. Schmidt, A. Wörner, J.J. H. u., O. Zabara, M. Fichtner, Int. J. Hydrogen Energy 36 (2011) 3556–3565.
[27] F.S. Yang, G.X. Wang, Z.X. Zhang, X.Y. Meng, V. Rudolph, Int. J. Hydrogen Energy 35 (2010) 3832–3840.
[28] J. Hu, M. Fichtner, Chem. Mater. 21 (2009) 3485–3490.
[29] G.A. Lozano, C.N. Ranong, J.M. Bellosta von Colbe, R. Bormann, J. Hapke, G. Fieg, T. Klassen, M. Dornheim, Int. J. Hydrogen Energy 37 (2012) 2825–2834.
[30] G.A. Lozano, J.M. Bellosta von Colbe, R. Bormann, T. Klassen, M. Dornheim, J. Power Sources 196 (2011) 9254–9259.
[31] F. Rouquerol, J. Rouquerol, K. Sing, Adsorption by Powders and Porous Solids: Principles, Methodology and Applications, Academic Press, London, 1999.
[32] B. Sakintuna, F. Lamari-Darkrim, M. Hirscher, Int. J. Hydrogen Energy 32 (2007) 1121–1140.
[33] O. Dolotko, N. Paulson, V.K. Pecharsky, Int. J. Hydrogen Energy 35 (2010) 4562–4568.
[34] E. Weidner, F. Dolci, J. Hu, W. Lohstroh, T. Hansen, D.J. Bull, M. Fichtner, J. Phys. Chem. C 113 (2009) 15772–15777.